Available online at www.sciencedirect.com
ScienceDirect
International Journal of Thermal Sciences 47 (2008) 1086–1095
International Journal of Thermal Sciences
www.elsevier.com/locate/ijts

Structural optimization of a microjet based cooling system for high power LEDs

Sheng Liu [a,b], Jianghui Yang [c], Zhiyin Gan [a,b], Xiaobing Luo [b,c,*]

[a] *Institute for Microsystems, School of Mechanical Engineering, Huazhong University of Science & Technology, Wuhan, China, 430074*
[b] *Wuhan National Lab of Optoelectronics, Huazhong University of Science & Technology, Wuhan, China, 430074*
[c] *School of Energy and Power Engineering, Huazhong University of Science & Technology, Wuhan, China, 430074*

Received 19 June 2007; received in revised form 10 September 2007; accepted 11 September 2007

Available online 31 October 2007

Abstract

Based on the previous experiments and simulations reported by the present authors, it was found the cooling system could be optimized to obtain better performance. In this paper, the microjet cooling systems with three different microjet structures were numerically investigated. The numerical model was proven by the experiments. The optimization results demonstrate that the microjet structure with one single inlet but two outlets can achieve better cooling performance. The simulation results show that the maximum temperature of the LED substrate cooled by the optimized microjet cooling device was 23 K lower than that of the LED substrate cooled by the present experimental cooling system.

Keywords: High power LED; Microjet cooling system; Numerical simulation; Structural optimization

1. Introduction

High power light emitting diode (LED) based semiconductor illumination technology, also called solid state lighting (SSL), has become the focus for both research and commercial applications in recent years, because it has a lot of advantages compared with the traditional illumination technologies. Currently, the major general light sources are incandescent lamps, halogen lamps, and fluorescent lamps. Compared with these general light sources, theoretically, LED has several advantages as follows [1]:

(1) high luminescence efficiency, good optical monochromaticity, narrow spectrum and being able to emit visible light directly;
(2) energy saving and low power consumption, as the power consumption of a LED is only one eighth of an incandescent lamp and one half of a fluorescent lamp under the same illumination efficiency and there is still potential to grow significantly in the next years to come;
(3) long lifetime; and
(4) being safe and environment-friendly.

In theory, LED's average lifetime is as long as 100 000 hours, which is ten times that of general lamps. LED is a solid state light source and has low calorific value and no thermal radiation, so that LED is generally called cool light source. In addition, LED does not contain any health hazard such as mercury, sodium, etc., and is recyclable and does not cause any pollution. Because of the above mentioned advantages, LEDs begin to play an important role in many applications [2]. Typical applications include back lighting for cell phones and other LCD displays, interior and exterior automotive lighting, large signs and displays, and are soon going to include general lighting such as street lighting and even the headlamps.

For present LEDs, especially for high-brightness LEDs, both optical extraction and thermal management are critical factors for the high performance of LED packaging. Most of the electrical power in LEDs will be converted into heat for the state of art technology with low internal and external optical extraction efficiency. In general, the produced heat will greatly

* Corresponding author. Tel.: +86 13971460283; fax: +86 27 87557074.
E-mail address: luoxb@mail.hust.edu.cn (X. Luo).

1290-0729/$ – see front matter
doi:10.1016/j.ijthermalsci.2007.09.005

reduce device luminosity. In addition, the high junction temperature will shift the peak wavelength of LED, thus changing the light color of LED. Narendran and Gu [3] have experimentally demonstrated that the life of LEDs decreases with increasing junction temperature in an exponential manner. Therefore, low operation temperature is strongly needed for LEDs, which is a distinguishing feature of SSL versus traditional lighting. Since the market requires that LEDs have high power and packaging density, it poses a contradiction between the power density and the operation temperature, especially when applications demand LEDs to operate at full power or more to obtain desired brightness. The problem leads to the emergence of major advances in thermal management of LED illumination.

To address the thermal problem of LEDs, numerous researchers both in China and in other countries have conducted the relevant studies. Arik and Weaver [4] carried out a numerical study to understand the chip temperature profile due to the bump defects. Finite element techniques were utilized to evaluate the effects of localized hot spots at the chip active layer. Sano et al. [5] reported an ultra-bright LED module with excellent heat dissipation characteristics. The module consists of an aluminum substrate having outstanding thermal conductivity and a mount for LED chips being formed into fine cavities with high reflectance to improve light recovery efficiency. Furthermore, the condenser of this LED module is filled with high-refraction index resin on the basis of optical simulation. An improvement in luminance of 25% or more was observed by taking the aforementioned measures in their paper. Petroski [6] developed a LED-based spot module heat sink in a free convective cooling system. Cylindrical tube, longitudinal fin (CTLF) heat sink is used to solve the orientation problem of LED. Chen et al. [7] presented a silicon-based thermoelectric (TE) for cooling of high power LED. The test results show that their TE device can effectively reduce the thermal resistance of the high power LED. Hsu et al. [8] reported a metallic bonding method for LED packaging to provide good thermal dissipation and ohmic contact. Zhang et al. [9] used multi-walled carbon nanotubes and carbon black to improve the thermal performance of thermal interface materials (TIM) in high-brightness LED packaging. Tests show that such a TIM can effectively decrease the thermal resistance. Acikalin et al. [10] used piezoelectric fans to cool LEDs. Their results show that the fans can reduce the heat source temperature by as much as 37.4 °C. The piezoelectric fans have been shown to be a viable solution for the thermal management of electronic component and LED.

In China, a lot of researchers have also tried to find the solutions to the LED thermal management. Wu et al. [11] used finite element method to analyze the temperature distribution in one watt high power white LEDs. The simulation results show good agreement with the experimental data. Based on the simulation model, they studied the dependence of chip size on the junction temperature. The results show that with a certain lighting efficiency and packaging structure, the size and maximum input power of chip should be optimized because of the thermal dissipation limit. Yu and Li [12] analyzed the dependence of bonding materials on the thermal characteristics of high power LEDs. They established a correlation of bonding material thickness with thermal conductivity and thermal resistance for flip-chip type LEDs. Examples with three typical materials are provided to prove the function. The results show that the bonding material plays an important role for decreasing LED thermal resistance. Chen and Song [13] utilized the thermal resistance model to predict the junction temperature and guide the thermal design of high power LEDs. By comparing with experiments, the feasibility of the model was proven. Ma and Bao [14] introduced a novel electrical measurement method for thermal resistance and junction temperature of high power LED. They also investigated the influence factors and constructed an experiment setup, and the experimental results show that the method has the advantages of simple structure and good stability. It can be used to measure thermal resistance and junction temperature of high power LEDs. Wang et al. [15] came up with an equation, which established the relation of LED output power with thermal characteristic parameters under transient condition. Based on the equation, the dependence of the LED output power on different current pulses was analyzed. The variation of optical output and heat with pulse width and duty ratio was presented.

Because of high power density of the LED array modules and systems, an active cooling solution, a microjet based cooling system was proposed for LED thermal management. About the cooling system, Liu's group [16,17] already conducted series of studies. They studied its performance for the thermal management of the high power LEDs which were less than 10 W. In the preliminary experiments [16], the temperature was measured by an infrared thermometer. Only the LED surface temperature was obtained, which should be different from the junction temperature of LED chips. In the enhanced investigations [17], several thermocouples were packaged into the chip substrate to conduct on-line temperature measurement and evaluate the cooling performance of the proposed system. Numerical simulations were also provided. The experimental and numerical results demonstrated that the microjet-based cooling system has good cooling performance.

In this paper, the microjet cooling system for a 220 watts LED light source was investigated. Different from the previous work in which the power of LED packaging was less than 10 watts, the present work studied a microjet cooling system for a 220 watts LED light source. Because of much larger power density, design of the present microjet device was more complicated. Experimental investigation on the thermal characteristics of the 220 watts LED light source was conducted. To understand the internal flow and heat transfer characteristics of its cooling device, circumstantial numerical simulations were also conducted. The numerical model was proven by the comparison with experimental results. After checking the feasibility of the simulation model, it was used to simulate and optimize the microjet device structures. Three kinds of structures were investigated and compared, an optimized microjet structure was found that compared well with the present experimental one.

2. Microjet array cooling system

Fig. 1 illustrates the proposed close-looped LED cooling system. It is composed of three parts: a microjet array device, a

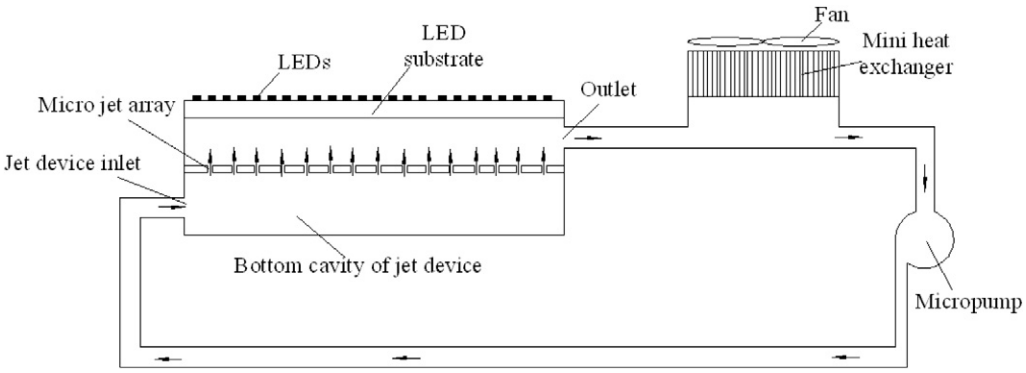

Fig. 1. Principle schematic of the microjet cooling system.

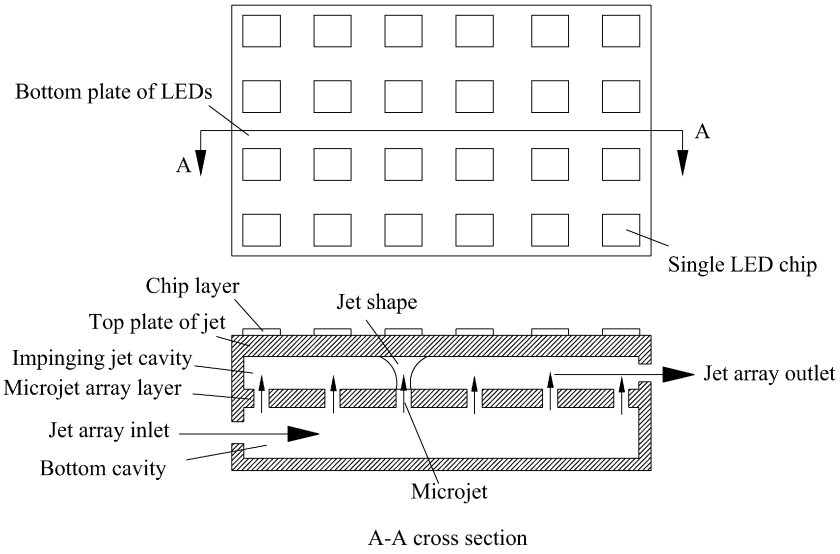

Fig. 2. Microjet array device.

micropump and a mini fluid container with a heat sink. When the LED needs to be cooled, the system is activated. Water or other fluids or gases in the close-looped system are driven into the microjet array device through an inlet by a micropump. Many microjets will form inside the jet device, which are directly impinged onto the bottom plate of the LED array. Since the impinging jet has a very high heat transfer coefficient, the heat created by the LEDs is easily removed by the recycling fluid in the system. The fluid is heated and its temperature increases after flowing out of the jet device, and then the heated fluid enters into the mini fluid container. The heat sink, which has a fan on the fluid container, will cool the fluid and the heat will be dissipated into the external environment. The cooled fluid is delivered into the jet device to cool the LED array, again driven by the force of the micropump in the system. The above processes constitute one operation cycle of the total system. It should be noted here that the real size of the proposed system can be designed as one small package according to the requirements of the application.

Fig. 2 shows the structure of the jet device of Fig. 1 in detail. It consists of several layers, which are (from top to bottom) the chip array layer, the top plate of the jet cavity, the impinging jet cavity, the microjet array layer and the bottom cavity. Cooled fluid enters into the device through the inlet, which is open at one side of the bottom cavity layer. The fluid flows through the microjet array and forms many microjets, as shown in Fig. 2. With sufficient driving force, the jets will impinge onto the top plate of the jet cavity which is bonded with the chip substrate of the LEDs. The heat conducted into the top plate of the jet cavity through the LED chips will be dissipated into the cooled fluid quickly due to the high heat transfer efficiency of the impinging jet. The fluid temperature increases and the heated fluid flows out from the jet array outlet, which is open at one side of the top jet cavity layer. Through this process, the heat from the LED chips will be transferred into the fluid efficiently.

3. Preliminary experiments

3.1. System and temperature measurement

The experimental system was constructed as shown in Fig. 3. The details of the microjet device were demonstrated in Fig. 4. To understand the thermal performance of the 220 watts LED light source cooled by the microjet device, the temperatures of the silicon gel which was coated on the chips were measured. The positions of the thermocouples were at the center part of

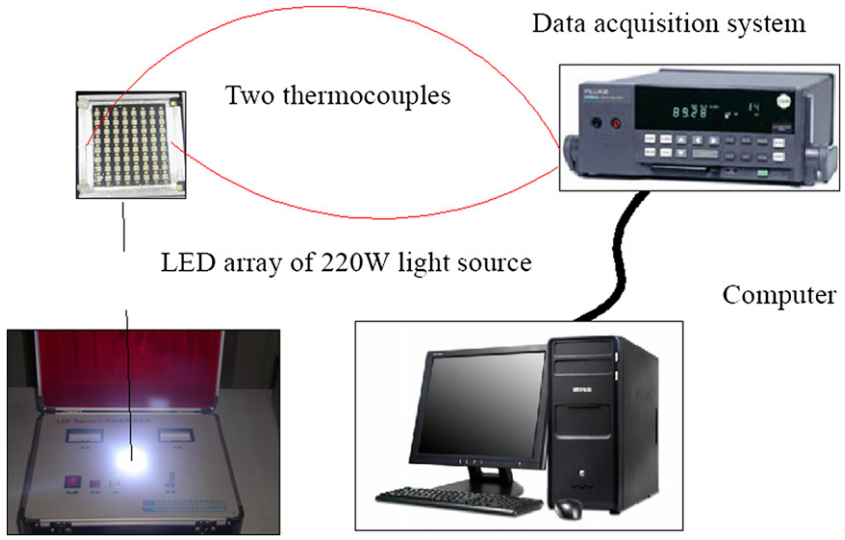

Fig. 3. Experimental system setup.

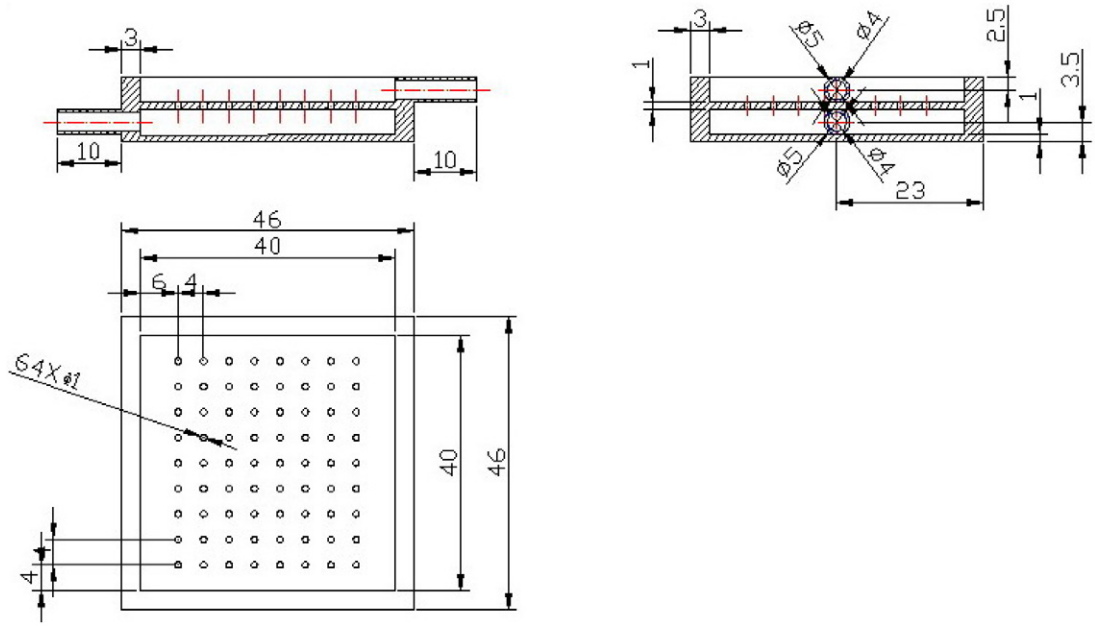

Fig. 4. Sizes of the microjet array in experiment (all dimensions are in mm).

the light source frame, as shown in Fig. 3. The working media of the cooling system was water. The light source frame was used to support the glass coated with phosphor. It is directly connected with the LED substrate by soldering. Since the thermal resistance between LED substrate and the frame was very small, the measured temperature can represent the LED substrate temperature. The data obtained by the thermocouples was transferred to the data acquisition system and displayed on the notebook monitor. The model of the data acquisition system in the experiment was Keithley 2700 multimeter and control unit 7700. It has 20 channels to collect data synchronously. However, in the present experiments, two thermocouple were just used, therefore, two channels of the data acquisition system were used.

3.2. Measurement accuracy

In the experiments, temperature was the main parameter for system evaluation, and its values at various locations were directly measured by thermocouples. The errors associated with temperature measurement mainly included measurement error of the thermocouples and reading error of the digital multimeter.

Standard T-type thermocouples (Cu–CuNi) were used in the experiments for temperature tests. During the temperature range from −30 °C to 150 °C, their measurement error was about 0.2 °C, its relative measurement error was about 0.75%. The data acquisition system had a reading error of 1 °C and 1% relative measurement error since the cold junctions of

the thermocouples used the default setup supplied by the system, not the ice bath with constant 0 °C. Therefore, the total error of the temperature measurement for the experiments was about 1.2 °C, and the relative measurement error was about 1.75%.

3.3. Experimental results

Fig. 5 shows the experimental results. In the experiments, the environment temperature was about 30.8 °C, the flow rate of the cooling system was about 18.5 mL/s, the working media was water. It can be observed from Fig. 5 that as the input power increases, the temperature of LED substrate increases quickly. When the input power is 227 W, its corresponding heat flux is about 14.18 W/cm^2, the temperature is about 69 °C. This simple test demonstrates that the LED light source cooled by the present system has low risk for temperature reliability since the maximum endurable temperature of the LED chip in the experiment is about 120 °C.

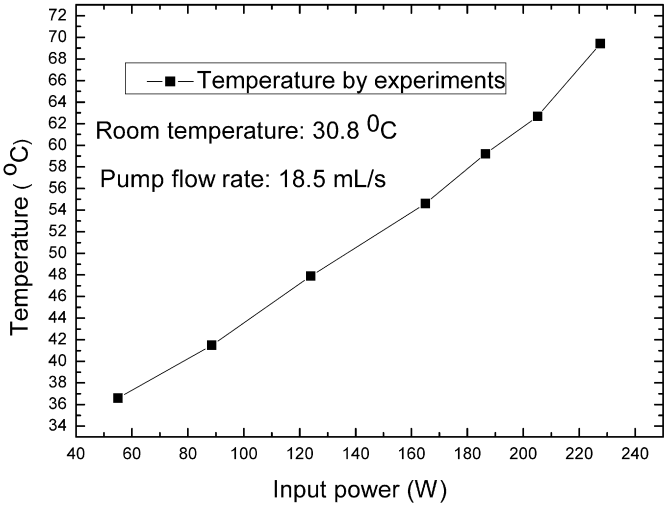

Fig. 5. Temperature variation with input power of the light source.

4. Simulation and model verification

It is necessary to compare simulation results with experimental results in order to verify the simulation model before using the model to conduct optimization. Commercial computational fluid dynamics (CFD) code FLUENT was used to build the numerical model. Fig. 6 demonstrates the simulation model of the microjet device, the structure of the microjet device in the experiment is exhibited by three figures acquired from three different views. The model parameters such as working conditions and sizes were exactly the same as those in the experiments. The diameters of the inlet and the outlet were 4 mm, the microjets were eight by eight array, the diameter of each microjet was 1 mm, the heights of impinging jet cavity and bottom cavity were 5 mm. Other parameters were shown in Fig. 4. It was a steady, incompressible and turbulent flow since the Reynolds number based on the inlet was about 7360. Standard k–ε model was used for turbulence simulation. First-order upwind method was used for the discretization of the governing equations. The Reynold time-averaging governing equations were as follows:

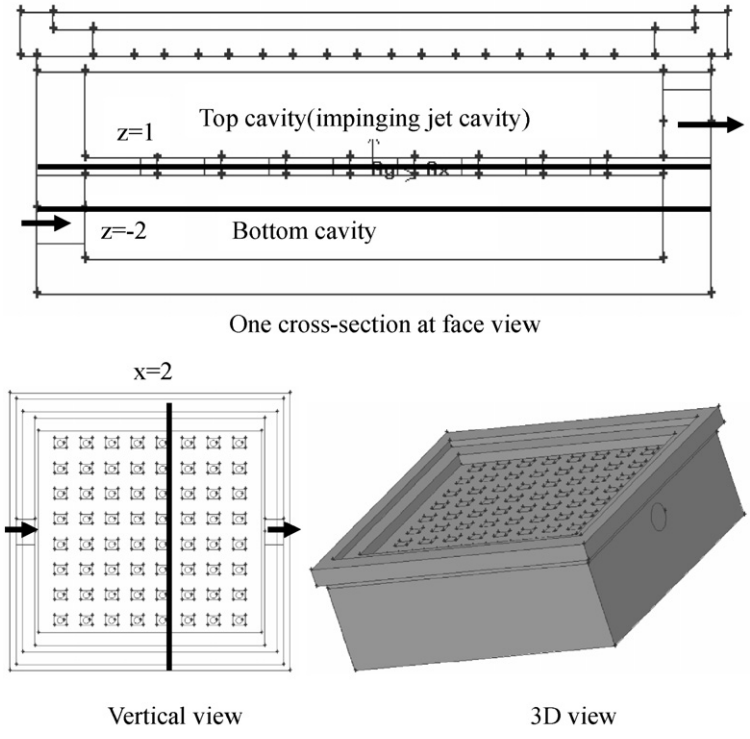

Fig. 6. Numerical model.

- Equation of continuity:

$$\frac{\partial \bar{u}}{\partial x}+\frac{\partial \bar{v}}{\partial y}+\frac{\partial \bar{w}}{\partial z}=0$$

- Equations of momentum:

$$\rho\left(\bar{u}\frac{\partial \bar{u}}{\partial x}+\bar{v}\frac{\partial \bar{u}}{\partial y}+\bar{w}\frac{\partial \bar{u}}{\partial z}\right)=-\frac{\partial \bar{p}}{\partial x}+\frac{\partial}{\partial x}\left(\mu\frac{\partial \bar{u}}{\partial x}-\rho\overline{u'^2}\right)+\frac{\partial}{\partial y}\left(\mu\frac{\partial \bar{v}}{\partial y}-\rho\overline{u'v'}\right)+\frac{\partial}{\partial z}\left(\mu\frac{\partial \bar{w}}{\partial z}-\rho\overline{u'w'}\right)$$

$$\rho\left(\bar{u}\frac{\partial \bar{v}}{\partial x}+\bar{v}\frac{\partial \bar{v}}{\partial y}+\bar{w}\frac{\partial \bar{v}}{\partial z}\right)=-\frac{\partial \bar{p}}{\partial y}+\frac{\partial}{\partial x}\left(\mu\frac{\partial \bar{u}}{\partial x}-\rho\overline{u'v'}\right)+\frac{\partial}{\partial y}\left(\mu\frac{\partial \bar{v}}{\partial y}-\rho\overline{v'^2}\right)+\frac{\partial}{\partial z}\left(\mu\frac{\partial \bar{w}}{\partial z}-\rho\overline{v'w'}\right)$$

$$\rho\left(\bar{u}\frac{\partial \bar{w}}{\partial x}+\bar{v}\frac{\partial \bar{w}}{\partial y}+\bar{w}\frac{\partial \bar{w}}{\partial z}\right)=-\frac{\partial \bar{p}}{\partial z}+\frac{\partial}{\partial x}\left(\mu\frac{\partial \bar{u}}{\partial x}-\rho\overline{u'w'}\right)+\frac{\partial}{\partial y}\left(\mu\frac{\partial \bar{v}}{\partial y}-\rho\overline{w'v'}\right)+\frac{\partial}{\partial z}\left(\mu\frac{\partial \bar{w}}{\partial z}-\rho\overline{w'^2}\right)$$

- Equation of energy:

$$\rho c_p\left(\bar{u}\frac{\partial \bar{t}}{\partial x}+\bar{v}\frac{\partial \bar{t}}{\partial y}+\bar{w}\frac{\partial \bar{t}}{\partial z}\right)=\frac{\partial}{\partial x}\left(\lambda\frac{\partial \bar{t}}{\partial x}-\rho c_p\overline{u't'}\right)+\frac{\partial}{\partial y}\left(\lambda\frac{\partial \bar{t}}{\partial y}-\rho c_p\overline{v't'}\right)+\frac{\partial}{\partial z}\left(\lambda\frac{\partial \bar{t}}{\partial z}-\rho c_p\overline{w't'}\right)$$

For the fluid inlet, the boundary condition of constant flow rate was adopted. The heat transfer coefficients of the natural convection boundary were 5 W/(m^2 K), which was used based on the authors' previous experimental tests. The system flow rate was 18.5 mL/s.

A study of the convergence of the grids was conducted before the calculation. The grids were refined until the flow field changed by 0.1%. Finally, a mesh of 1 321 262 grids was used in the simulation. The gird number of each microjet was about 25. The residual controls of the energy equation and continuity equation were 1E−9 and 1E−3.

Fig. 7 shows a comparison between the temperatures in the experiments and simulations. Here the pump flow rate was 18.5 mL/s, and the input power of the LEDs was variable, the working media was water. In this comparison, the temperature sampling positions in experiments and simulations were exactly the same. It can be seen from Fig. 7 that seven different input powers were used. The simulation temperatures were close to the measured values at the input powers of 55, 88.5, 124 and 227.5 W. However, the temperature differences between the experiments and simulations at the input powers of 165, 186.5 and 205.2 W were much larger than those at the other four input powers. They were 2.2, 3.2 and 3.2 °C respectively. Correspondingly, the errors of the simulations compared with the experiments at these three input powers were about 3.71%, 5.42% and 5.1%. Thus, the maximum error between experiments and simulations in Fig. 8 was 5.42%. The difference between the simulation and the experiments can be explained as following. In the experiments, water in the loop was not boiled to remove the gas dissolved inside, but in the simulation, the working media was pure water. The simulation case was ideal

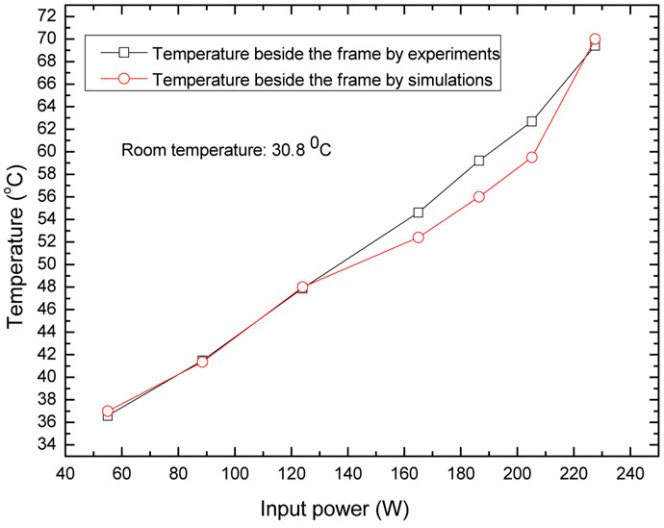

Fig. 7. Temperature comparison between experiment and simulation.

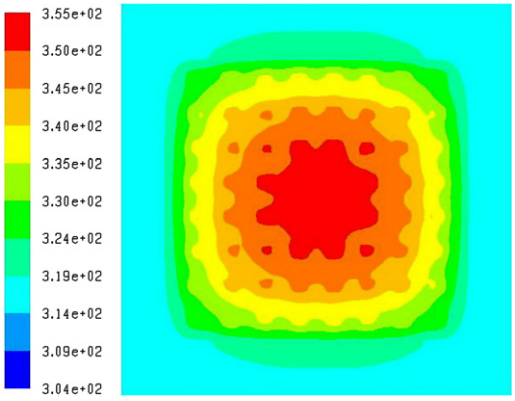

Fig. 8. Temperature distribution of LED substrate.

one compared with the experimental conditions. Based on the above comparison and analysis, it was found that this model could be used for simulation and further analysis.

5. Comparison and optimization of three microjet devices

Simulation was used to compare the temperature and flow distribution in three kinds of different microjet devices. To compare them effectively, all simulation conditions except the structure sizes were the same.

5.1. Flow and temperature distributions inside the microjet device used in the above experiments

The simulation model in this case is shown in Fig. 6. Based on this model, the temperature distribution of the microjet device used in the experiment was achieved and shown in Fig. 8 when the input power was 220 watts and the corresponding heat flux was 13.75 W/cm^2. From Fig. 8, it can be seen that the temperatures of the LED substrate at the centre zone of the microjet device are the highest, the maximum temperature is 355 K (81.9 °C).

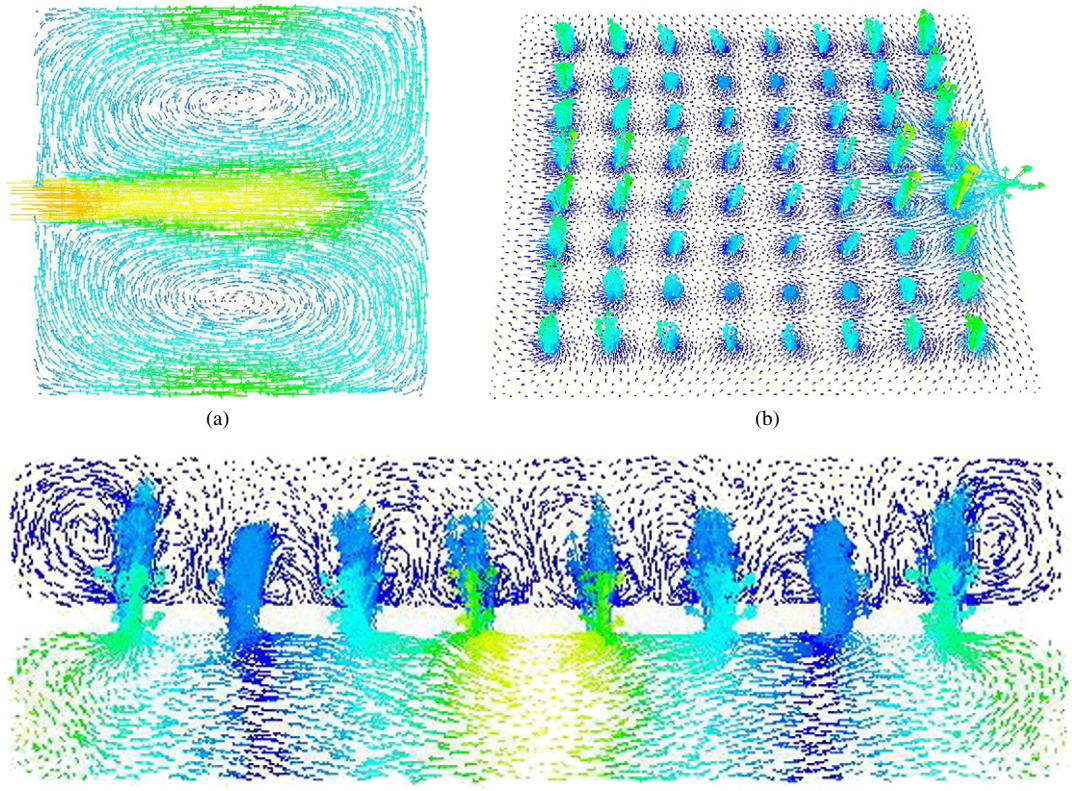

Fig. 9. (a) Flow distribution at the cross-section of $z = -2$. (b) Flow distribution at the cross-section of $z = 1$. (c) Flow distribution at the cross-section of $x = 2$.

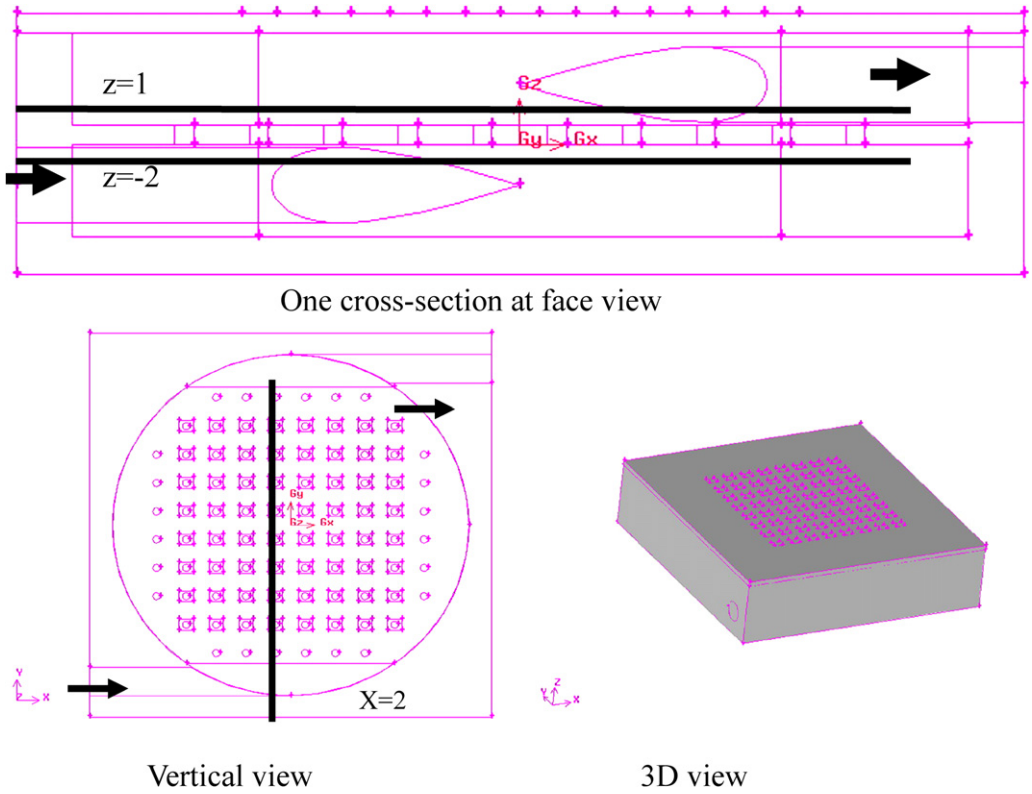

Fig. 10. Simulation model of an improved microjet device.

Flow field distributions in the microjet device are shown in Fig. 9. From Fig. 9(a), it is clear that there are two vortexes in the bottom cavity when the fluid enters into the bottom cavity through the inlet. When the fluid flows through the microjets, the impinging jets are formed as shown in Figs. 9(b) and (c). The flow in the top cavity (or impinging jet cavity shown in Fig. 6) is disturbed strongly. However, because of the vortexes in the bottom cavity, as shown in Fig. 9(c), the velocities of the impinging jets at the centre part of the microjet device are much smaller than those of jets at the edge part of the microjet device, which results in that the heat transfer at the centre zone of the microjet device is weaker compared with those at the other parts. Such a flow distribution clearly explains the reason for that the chip temperatures at the centre zone were the highest.

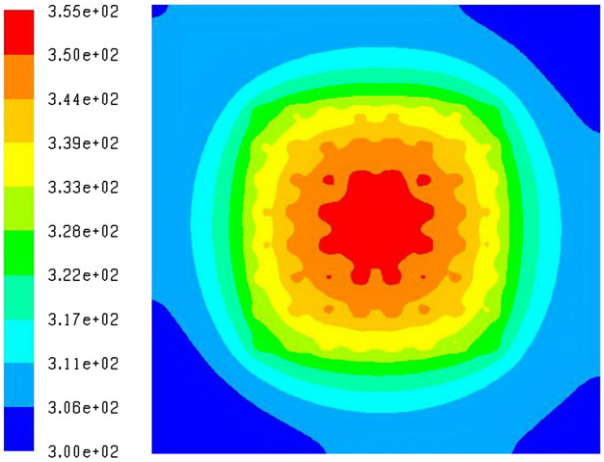

Fig. 11. Temperature distribution of LED substrate.

5.2. Flow and temperature distribution for an improved microjet device

The simulation model of an improved microjet device is shown as Fig. 10. The similarity between the current microjet device and the one in the experiments was that it also had single inlet and single outlet, the diameters of the inlet and the outlet channel were 4 mm. What was different from the above-studied microjet device was that the shape of impinging jet cavity and bottom cavity was cylinder whose height was 5 mm. Because of shape change, the distribution of the microjets was different from that of the experimental model, 88 microjets whose diameter was 1 mm were uniformly distributed as shown in Fig. 10.

In this simulation, total mesh number was 540 338, the turbulence model was standard k–ε model, velocity inlet and pressure outlet were the inlet and outlet boundary conditions respectively.

The temperature distribution is shown as Fig. 11. It is seen that the temperature of the LED substrate at the centre zone is the highest, which is 355 K (81.9 °C). This is the same as that in the experimental model, and it demonstrates that the cooling performance of the present microjet device does not show much improvement.

Flow field distributions in the cavity are shown in Fig. 12. It is clear from Fig. 12(a) that there is one big vortex in the bottom cavity; therefore, the jet velocities in the center part are much smaller than those in the edge part as shown in Figs. 12(b) and (c). Such a flow distribution will result in the non-uniform temperature distribution as shown in Fig. 11, where the temperatures at the center zone are much higher than those at the other zones.

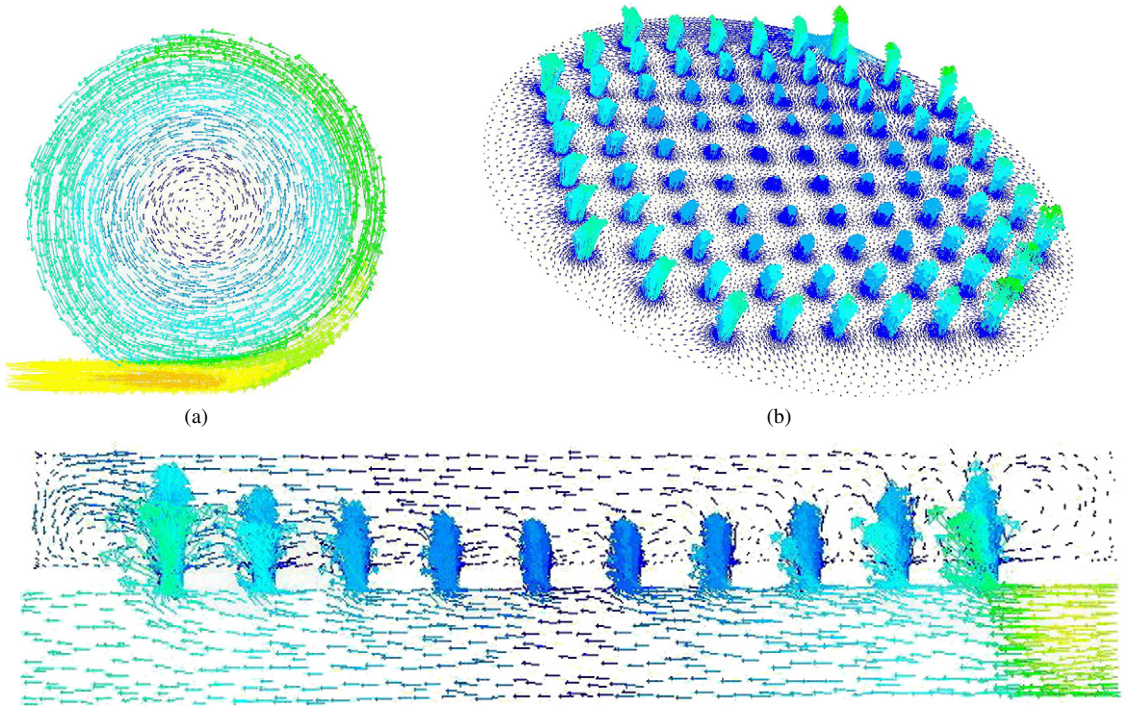

(a) (b)

(c)

Fig. 12. (a) Flow distribution at the cross-section of $z = -2$. (b) Flow distribution at the cross-section of $z = 1$. (c) Flow distribution at the cross-section of $x = 2$.

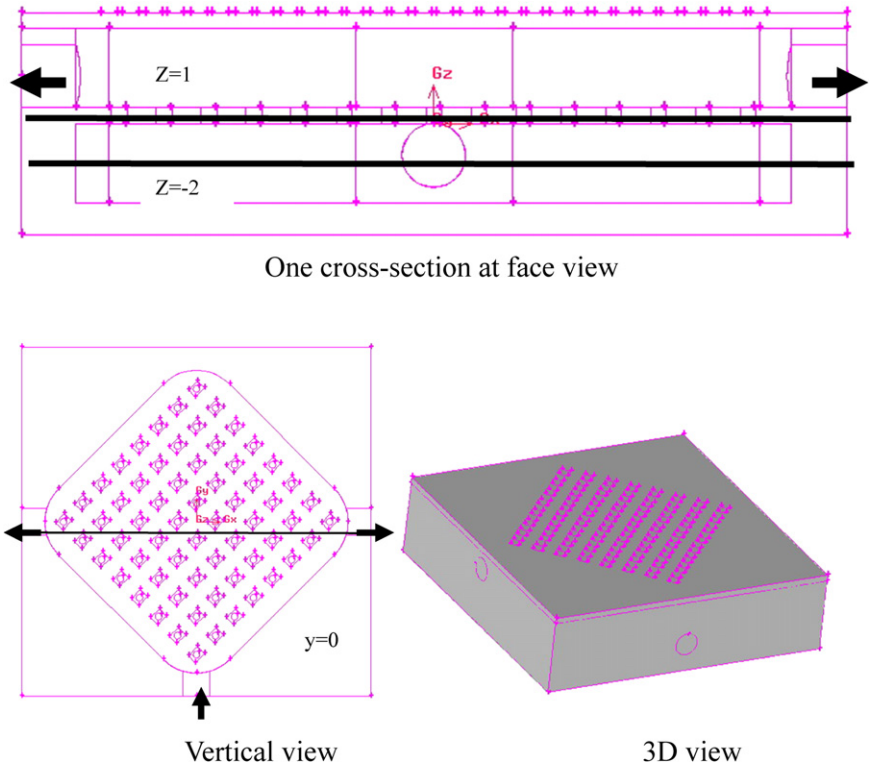

Fig. 13. Simulated model of the microjet device with one inlet and two outlets.

Obviously, compared with the experimental model, changing the shape of cavity like this case has little effect on improving the cooling performance. It is necessary to find other cavity structures to improve the flow distribution and achieve uniform temperature distribution.

5.3. *Flow and temperature distribution for another improved microjet device*

Another improved microjet system is shown in Fig. 13, which has one inlet but two outlets. The diameters of the inlet and the outlet were 4 mm. The shape of impinging jet cavity and bottom cavity was cuboids type whose height was 5 mm. The microjet array were composed of eight by eight microjets, and the diameter of each microjet was 1 mm.

In the simulation, the total mesh number was 591 841, other boundary and working conditions were the same as those described in the above two models. The steady temperature distribution is shown in Fig. 14. It is noted that the maximum temperature of the LED substrate is 332 K (58.9 °C), which is 23 K lower than those achieved in the above two models. This demonstrates that the present microjet device has better cooling performance compared with the above two designs.

The flow distributions in the microjet device are shown in Fig. 15. There are two vortexes in the bottom cavity as shown in Fig. 15(a). Even though, from Figs. 15(b) and (c), it can be seen that the impinging jets are much more uniform compared with those in the above two models, which tells the reason of relatively uniform temperature distribution shown in Fig. 14. From Fig. 15(c), it is also noted that turbulence in the top cavity

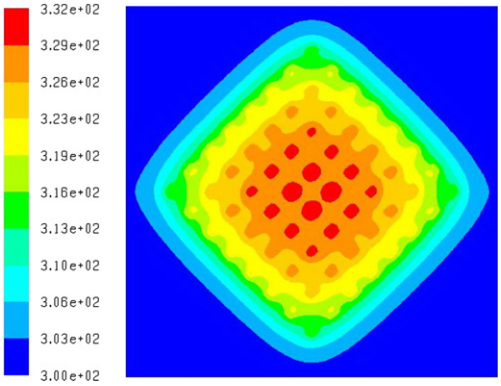

Fig. 14. Temperature distribution of LED substrate.

is much stronger than those in the above two models. Therefore, the maximum temperature of the LED substrate is 23 K lower as described in Fig. 14.

6. Summary

The microjet based cooling system for high power LED was investigated in this paper, which was a continuation of the previous work conducted by the authors' group. Through the preliminary experiments, the temperature distribution of LED substrate under different input power was achieved. To improve the cooling performance of the microjet device, simulation was conducted. The feasibility of the simulation model was proven by comparing the simulation result with the experiment ones. By such a simulation model, three kinds of microjet device were studied, their flow and temperature distributions were provided.

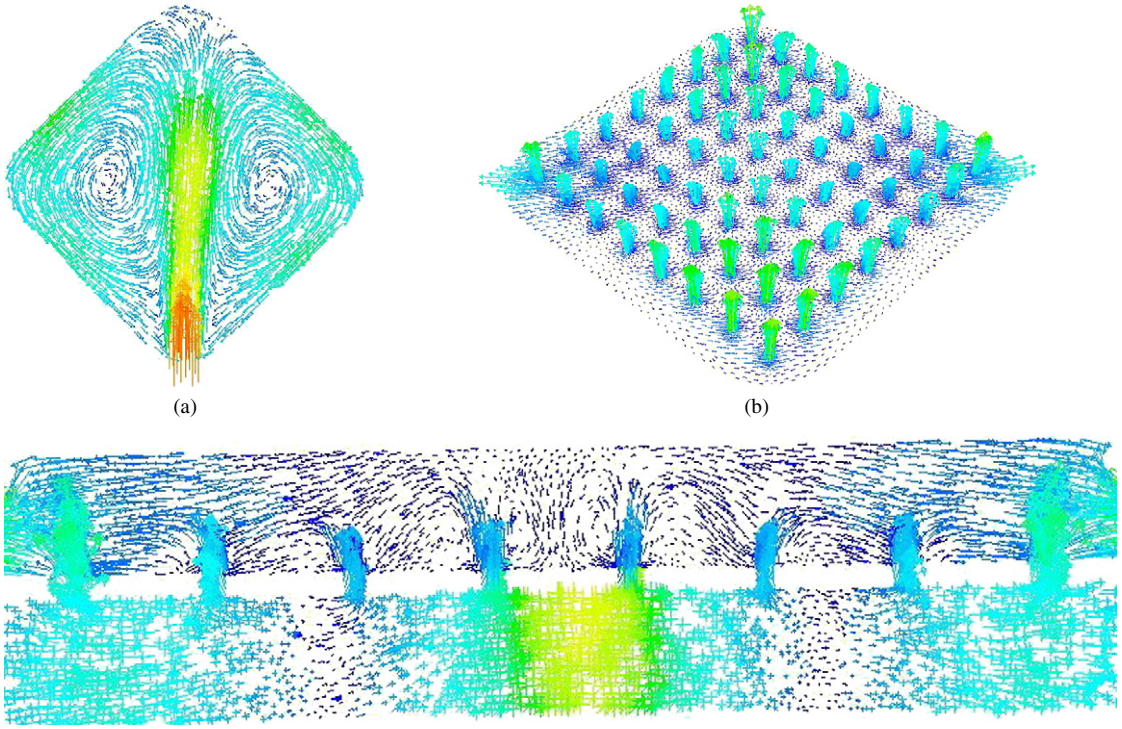

Fig. 15. (a) Flow distribution at the cross-section of $z = -2$. (b) Flow distribution at the cross-section of $z = 1$. (c) Flow distribution at the cross-section of $y = 0$.

The comparison results show that under the same conditions, the microjet device design with one inlet and two outlets can achieve the much better cooling performance. The maximum temperature of the LED substrate cooled by such a microjet device is 23 K lower than those cooled by the other two designs. The main reason for such an amelioration is that the flow distribution in the design is much more uniform, the averaging flow turbulence is much stronger.

Acknowledgements

We acknowledge the financial support from Key Technology R&D Program of Hubei Province, China (2006AA103A04). The authors also would like to provide appreciation to Mr. Wei Chen for his help in numerical simulations.

References

[1] A. Zukauskas, M.S. Shur, R. Gaska, Introduction to Solid-State Lighting, John Wiley and Sons, New York, 2002.
[2] M. Alan, Solid state lighting—a world of expanding opportunities at LED 2002, III–Vs Rev. 16 (2003) 30–33.
[3] N. Narendran, Y.M. Gu, Life of LED-based white light sources, IEEE J. Disp. Tech. 1 (2005) 167–171.
[4] M. Arik, S. Weaver, Chip scale thermal management of high brightness LED Packages, in: I.T. Ferguson, N. Narendran, S.P. DenBaars, et al. (Eds.), Fourth International Conference on Solid State Lighting, Denver, Colorado, USA, in: Proceedings of the SPIE, vol. 5530, SPIE, 2004, pp. 214–223.
[5] S. Sano, H. Murata, K. Hattori, Development of flat panel LED module with heat sink, Mitsubishi Cable Ind., Rev., 1993 (in Japanese).
[6] J. Petroski, Understanding longitudinal fin heat sink orientation sensitivity for Light Emitting Diode (LED) lighting applications, in: Proc. International Electronic Packaging Technical Conference and Exhibition, Maui, Hawaii, USA, 2003, pp. 111–117.
[7] J.H. Chen, C.K. Liu, Y.L. Chao, et al., Cooling performance of silicon-based thermoelectric device on high power LED, in: Proc. 24th International Conference on Thermoelectrics, Clemson, South Carolina, USA, University of Clemson, 2005, pp. 53–56.
[8] C.C. Hsu, S.J. Wang, C.Y. Liu, Metallic wafer and chip bonding for LED Packaging, in: Proc. the 5th Pacific Rim Conference on Lasers and Electro-Optics, vol. 1, Taipei, Taiwan, 2003, p. 26.
[9] K. Zhang, G.W. Xiao, C.K.Y. Wong, et al., Study on thermal interface material with carbon nanotubes and carbon black in high-brightness LED packaging with flip-chip, in: Proceedings of 55th Electronic Components and Technology, Orlando, Florida, USA, 2005, pp. 60–65.
[10] T. Acikalin, S.V. Garimella, J. Petroski, et al., Optimal design of miniature piezoelectric fans for cooling light emitting diodes, in: Proc. Ninth Intersociety Conference on Thermal and Thermomechanical Phenomena in Electronic Systems, vol. 1, New York, USA, 2004, pp. 663–671.
[11] H.Y. Wu, K.Y. Qian, F. Hu, Y. Luo, Study on thermal performances of flip-chip high power LEDs, J. Optoelectron. Laser 16 (2005) 511–514 (in Chinese).
[12] B.H. Yu, X.F. Li, Impact of flip chip substrate adhesive on the thermal characteristic of high power LED, Semicond. Technol. 30 (2005) 49–51 (in Chinese).
[13] Y. Chen, X.J. Song, Application of thermal resistance model in high power LED, China Illumination Equipment 7 (2005) 5–7 (in Chinese).
[14] C.L. Ma, C. Bao, A novel measuring method of thermal resistance for high power LED, Opt. Instrum. 27 (2005) 13–17 (in Chinese).
[15] Y.T. Wang, J.S. Shi, L.T. Wang, Analysis and calculation on junction LED thermal characteristics in engineering, Semicond. Optoelectron. 15 (1994) 143–146 (in Chinese).
[16] X.B. Luo, S. Liu, X.P. Jiang, T. Cheng, Experimental and numerical study on a micro jet cooling solution for high power LEDs, Sciences in China, Series E 50 (4) (2007) 478–489.
[17] X.B. Luo, S. Liu, A microjet array cooling system for thermal management of high-brightness LEDs, IEEE Trans. Adv. Packaging 30 (3) (2007) 475–484.